

Impact of surface roughness on Dielectrophoretically assisted concentration of microorganisms over PCB based platforms

Geeta Bhatt¹ · Rishi Kant¹ · Keerti Mishra² · Kuldeep Yadav¹ · Deepak Singh² · Ramanathan Gurunath² · Shantanu Bhattacharya^{1,3}

Published online: 17 April 2017
© Springer Science+Business Media New York 2017

Abstract This article presents a PCB based microfluidic platform for performing a dielectrophoretic capture of live microorganisms over inter-digitated electrodes buried under layers of different surface roughness values. Although dielectrophoresis has been extensively studied earlier over silicon and polymer surfaces with printed electrodes the issue of surface roughness particularly in case of buried electrodes has been seldom investigated. We have addressed this issue through a layer of spin coated PDMS (of various surface roughness) that is used to cover the printed electrodes over a printed circuit board. The roughness in the PDMS layer is generally defined by the roughness of the FR4 base which houses the printed electrodes as well as other structures. Possibilities arising out of COMSOL simulations have been well validated experimentally in this work.

Keywords PDMS · PCB · Inter-digitated electrodes · DEP · *E. coli*

1 Introduction

The advancements in Micro/Nano Systems (MEMS/NEMS) technology have always served as a tool for scaling down a

variety of structures which may serve mechanical or electrical purposes. The scaling down process is of utmost significance in biological world as some of the biological entities match size-wise with the scaled down structures and features. Due to this scale down effect there has been a revolution in clinical detection technology which has provided many solutions. One example could be the sensitive detection of pathogens in various food and water samples. There have been many strategies involved earlier through use of pre-concentration, selective recognition, molecular recognition, molecular identification etc. on single microchip platforms (Nayak et al. 2013). Dielectrophoresis (DEP) phenomena has been extensively used in microchip architectures for separating, concentrating, manipulating etc. of target samples from neutral solutions by use of non-uniform electric field. Further DEP force has been characterized very well numerically (Pohl 1951) and is found to depend on particle polarizability, dielectric properties of the particles and surrounding media and also particle size. In fact the average DEP force (Jones 1996), F_{DEP} for a spherical dielectric particle flowing in a medium is expressed as:

$$F_{DEP} = 2\pi r^3 \varepsilon_o \varepsilon_m \text{Re}[K(\omega)] |\nabla| E_{rms}|^2 \quad (1)$$

where, r is the radius of the particle, ε_o is permittivity of free space, ε_m is real part of the permittivity of medium, E_{rms} is RMS electric field and $K(\omega)$ is Clausius-Mossotti factor (measure of effective polarizability of the particle).

Clausius-Mossotti factor is expressed as:

$$K(\omega) = \frac{(\varepsilon_p^* - \varepsilon_m^*)}{(\varepsilon_p^* + 2\varepsilon_m^*)}; \quad (i = p, m) = \varepsilon_i - j \frac{\sigma_i}{\varepsilon_o \omega} \quad (2)$$

Here, m & p refers to the medium and particle, ε is permittivity, σ is conductivity and ω is angular frequency of applied

✉ Shantanu Bhattacharya
bhattacs@iitk.ac.in

¹ Microsystems Fabrication Laboratory, Department of Mechanical Engineering, Indian Institute of Technology, Kanpur, Kanpur, India

² Chemistry Department, Indian Institute of Technology, Kanpur, Kanpur, India

³ Design Program, Indian Institute of Technology, Kanpur, Kanpur, India

field ($\omega = 2\pi f$). The polarizability of suspended particles in a medium (magnitude and direction of DEP force) is dependent of the frequency and magnitude of applied electric field, dielectric constant and conductivity of media. DEP can be performed through electrodes or in an electrodeless manner. In DEP through electrodes (Voldman et al. 2002) depending on the size and spacing in the electrode geometry DEP can be performed at low voltages in miniscule sample volume whereas in electrodeless DEP very high voltages (Chou et al. 2002) are used. The utilization of this DEP phenomenon finds applications in manipulating particles, beads nanowires, biological entities like bacteria etc. The DEP force has been utilized intensively for various microfluidic applications like cell sorting (Lin and Lee 2008; Wang et al. 2013), cell separation (Hawkins et al. 2007), assembling (Freer et al. 2010; Collet et al. 2015), patterning and other applications. DEP is used to detect pathogenic bacteria (Ivnitski et al. 2000; Su and Li 2004) in extremely short time durations. DEP is also deployed to perform DNA capture which is highly dependent on capture frequency (Kasahara et al. 2015) of the input signal. Gold inter-digitated electrodes (IDEs) (Bakewell and Morgan 2006), castle-walled microelectrodes (Kasahara et al. 2015) and carbon nanotubes (Tuukkanen et al. 2006) are all used for capturing of DNA. It has been observed that below a certain cross over frequency, positive DEP is observed through capture in the inter-electrode gap region. This shifts to negative DEP with capture over the electrodes after the cross over frequency is exceeded. Various applications of DEP like particle sorting, cell manipulating and particle focusing are combined with other techniques of flow fractionation and electromediated lysis of cells to make an integrated platform for sample preparation and handling (Manuscript and Instruments 2009). Further a lot of analytical close form solutions have been proposed to model DEP (Nerguizian et al. 2012). DEP is also deployed in pure biological application for isolation, concentration and detection of DNA biomarkers and drug delivery nano-vehicles (nanoparticles) in blood samples (Sonnenberg et al. 2012). Both DNA and nanoparticles possess higher molecular weight as compared to blood cells and may undergo positive DEP which leads to their separation from blood cells. Electrode-less DEP has also been used for separating red blood cells from blood borne pathogens (*E.coli*) (Chang et al. 2007) by applying high input voltages in the range of 500 V_{pp}. A light induced biochip has also been reported (Wu et al. 2016) wherein capture of particles are carried out through light projection on silicon surfaces. Printed circuit Boards (PCBs) are also deployed for performing DEP based manipulation of cells as an inexpensive solution. In this context, Park et al. 2009 has shown DEP capture of cells on IDEs (width and spacing ≈ 152 or $229 \mu\text{m}$) made on PCBs. PCB technology is also used for manipulation of HeLa cells and polystyrene beads using high input voltage

of the range 76 V_{pp} at 1 MHz. Separation of beads and cells on PCB using multiple channels (Millet et al. 2011) is also carried out in case of laminar flow. Although various authors have investigated different aspects related to the physics of the DEP phenomena there is seldom any work reported on metrological aspects of the capture surface like surface topology and roughness and their impact in the capture process. As non-uniformity in the electric field is the principle reason to cause DEP, it must depend on the electric field localization over the capture surface particularly in rough surfaces. In this light, we have demonstrated the characterization of the base surface of a PCB board with patterned IDEs where the DEP phenomena is observed over the whole surface of fixed and varying surface roughnesses. A voltage i.e., 10 V_{pp} at frequency of 2 MHz is applied on IDEs which are buried inside a coating of polydimethyl siloxane layer (PDMS) layer of thickness 5–10 μm). A top mounted micro fluidic channel is made through replication and molding process and is bonded over the PDMS coated PCB. The impact of surface roughness is modeled in COMSOL 5.2 a; and also observed physically in terms of the capture phenomena. It is observed that the surface roughness is a critical factor that may determine the capture pattern on a surface of a given roughness.

2 Materials and methods

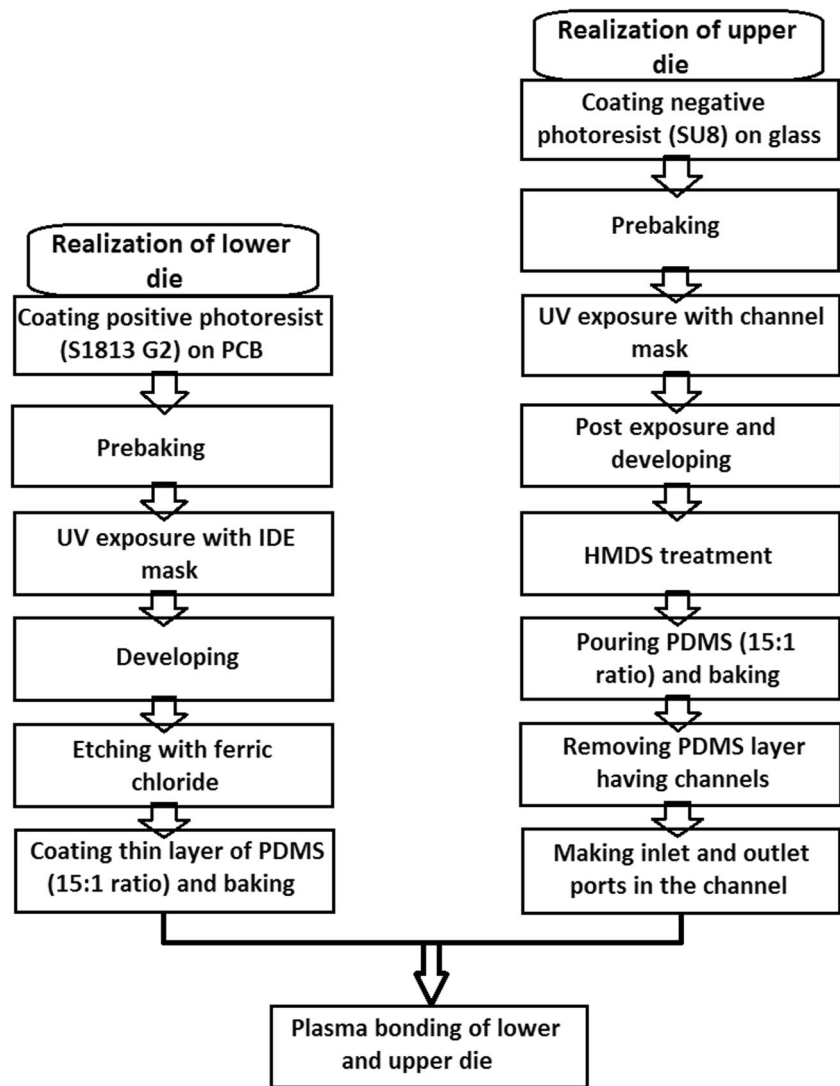
2.1 Micro-fluidic chip design and fabrication in PCBs

The microfluidic chip is made using standard PCB technology into two halves with the upper half being made in PDMS using replication and molding technique (McDonald et al. 2000) and the lower half being made over the PCB using standard photolithography and etching techniques (Nguyen and Huang 2001). Figure 1 details the fabrication flow chart.

2.1.1 Realisation of lower die

The lower die was made out of a PCB substrate sized about 1 sq. inch with an electroplated thick copper coating (thickness $\approx 17 \mu\text{m}$). The copper coating has been utilized through photo-patterning and selective chemical etching to realize the IDEs. The photoresist used was positive tone (S-1813, Microposit) and was eventually used as a sacrificial layer for performing the copper etching which was carried out with a 0.6 M anhydrous ferric chloride solution in DI water. The width of electrodes that was achieved in our experiments was 40 μm

Fig. 1 Flowchart showing fabrication steps of microfluidic chip



with an interelectrode gap of $55\ \mu\text{m}$ [Refer Figs. 2 (d)]. Further controlled etching of patterned electrodes was done in a manner to achieve electrode thickness of $\approx 6\ \mu\text{m}$ (same thickness considered for simulations also). The electrodes patterned on the PCB layer were masked using a layer of black paint (to prevent background fluorescence cropping up from the FR4 layer). Another layer of Polydimethyl siloxane of thickness $5\text{--}10\ \mu\text{m}$ controllable through spinning with speeds varying between 4500 and 5000 rpm was coated on the chip. The patterned electrodes were further characterized using 3D optical profilometry on a ContourGT (M/s BRUKER) and observations were carried out prior and after coating. The surface topology and roughness observations of the PDMS coated surface were imported into the geometry module of COMSOL and the electric field variability over the surface contour was closely modelled [Details in section 3.1].

2.1.2 Realisation of upper die

The upper die was made using the replication process over a mold which contained a photo-patterned negative of the micro-channels. The channel width that was replicated was around $225\ \mu\text{m}$ and the depth was around $10\text{--}15\ \mu\text{m}$. Hexa methyl disiloxane (HMDS) was used as a mold release agent on the glass patterned negative of the microchannels. After making the PDMS replica, inlet/outlet ports were punctured in the channel layer (Hole size $\approx 500\ \mu\text{m}$).

2.1.3 Assembly of lower and upper die

Both the upper and lower dies were bonded to each other irreversibly using plasma oxidation through a PD 32G (M/s Harrick plasma). The dies were aligned under an optical microscope in a manner so that the channels were overlaid on the printed IDEs on the lower die.

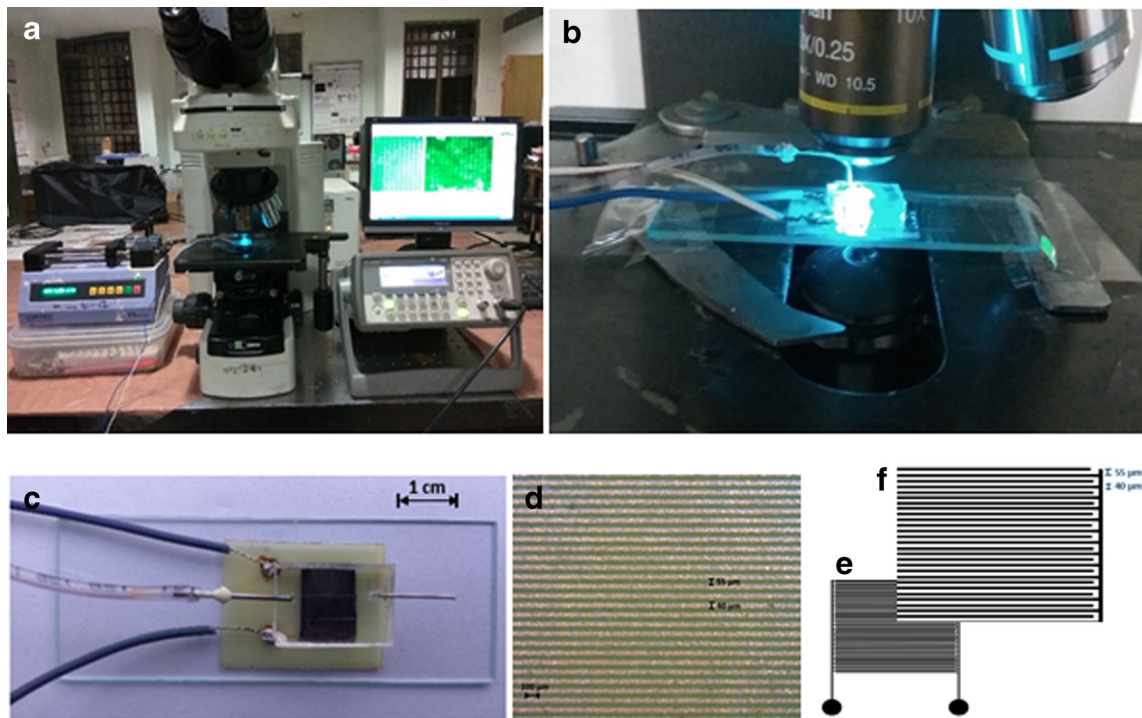


Fig. 2 Experimental entities. **a** Complete experimental set up; **b** Chip with DEP capture taking place under fluorescence microscope; **c** fabricated chip used for carrying out DEP capture; **d** Etched electrodes

on the PCB; **e** Mask pattern design and **f** Closer view of a portion of actual mask used for doing lithography

2.2 COMSOL simulation

COMSOL simulations with imported roughness from profilometry data containing information related to surface topology and roughness has been used for simulating the DEP based capture process of the particles. The simulation is carried out on particles of size 2 μm being captured between two consecutive electrodes. The governing equations (Eqs. 1–3) as well as boundary conditions (Eqs. 4–6) are represented in Eqs. 1–6.

Particle velocity after being experienced by the dielectrophoretic force,

$$\frac{d(m_p v)}{dt} = F_{DEP} \tag{3}$$

where, m_p is density of particles.

At inlet, left most boundary,

$$\text{Inlet velocity, } v_o(\text{at } x=-10) = 1 \times 10^{-4} \text{ m/s} \tag{4}$$

At outlet, right most boundary,

$$\left. \begin{array}{l} \text{Outlet velocity, } v(\text{at } x=145) \text{ (from equation (3))} \\ \text{Wall condition : freeze} \end{array} \right\} \tag{5}$$

$$\text{Upper boundary insulated, } q(\text{at } y=17) = 0 \tag{6}$$

The simulations are performed on 10 particles flowing into the chip in a time space of 0.035 s. The applied electric

potential of 10 V_{pp} is provided to stimulate the electrodes and a DEP assisted particle manipulation approach is used for tracing the particles in the spatial variation of electric field. Simulations are carried out in the presence and absence of the surface induced roughness brought in from the profile-metric observations and the DEP effects are studies and reported in details below. Mesh size optimization is carried out with respect to the no. of capture events and the mesh size is varied upto a minimum element size of 0.01 μm. The properties of various matters used in simulation are tabulated in Table 1.

The capture pattern is generated for a total time of 3 s in both the cases (i.e., with roughness and without roughness) and the results are compared as detailed later.

2.3 Experimental set up

The DEP capture of *E. coli* DH5α cells was performed as validation to establish the surface roughness effect of the PDMS spun coated layer on the capture process. *E. coli* DH5α cells were stained with Acridine Orange (1 × 10⁻⁶ M) for easy visualization with an inverted fluorescence microscope (Nikon ECLIPSE 80i, Japan) top mounted with a charged coupled device (CCD) camera (Media cybernetics). An excitation signal of wavelength 540–565 nm was generated using a band pass filter for visualizing the stained and captured cells and the emission was monitored over 605–660 nm range using a TRITC

Table 1 Properties of materials used in the simulation

Material	Density (Kg/m ³)	Relative permittivity	Poisson's Ratio	Electrical Conductivity (S/m)	Diameter (μm)
Copper (Electrode material)	8960	1	0.355	5.998×10^7	
Water (Fluid in which particles are dispersed)	1000	80.1		5.5×10^{-6}	
Poly Dimethyl Siloxane (PDMS) (Mark 1999) (Material coated on electrodes)	0.97	3.5	0.5	2.5×10^{-14}	
Particles (<i>E. coli</i>) (Martinez-Salas et al. 1981, Bai et al. 2006)	1105	100		0.22	2

filter. The CCD camera was used for capture the fluorescence images of the DEP assisted capture process of the microorganisms inside the micro-channels. Further the DEP capture was monitored by flowing in different solutions with varying cellular concentrations (9.25×10^7 , 6.95×10^7 , 5.8×10^6 and 4.5×10^4). As detailed in the fabrication step a black coat of paint is deliberately made in the lower die to cover the etched electrodes to prevent background fluorescence. The stained cells were flown in the channel through a 5 ml syringe with the help of a Syringe pump (11PLUS HARVARD apparatus) at a flow rate of 5 μl/h. For carrying out the DEP assisted capture, an input voltage of 10 V_{pp} was provided at 2 MHz frequency using an arbitrary waveform generator (Agilent 33220 A). Figure 2 shows the image of experimental set up.

2.4 Bacterial strain

The *E. coli* DH5α cells were transformed with PET28a vector (M/S Bangalore Genei) containing a DNA insert of 927 base pairs. The colonies were grown on Kanamycin plates as the plasmid vector PET28a imparts resistance against Kanamycin. The cells were grown in Luria Bertani (LB) (M/S Bangalore Genei) media for approximately 12–14 h in a shaking incubator (M/S Mahendra Scientific, India) at 37 °C till the solution reaches the OD of around 2.0 at 600 nm. The cells were then extracted at 4 °C, 4500 rpm for 15 min through centrifugation process (Centrifuge 5804 R, Eppendorf Germany). The cells were further washed with 4–5 times with Phosphate buffer saline (1× solution) and then are suspended in Milli Q water. The transformant was merely used to study the effect of DEP on cell viability as the confirmation of live cells after DEP assisted capture was obtained through plate culture and growth technique.

E. coli DH5α cells were stained with Acridine Orange by simple mixing with Acridine Orange solution (1×10^{-6} M) with the cellular suspension in 1:1 ratio followed with an incubation of 5 mins. The stained cells were washed thrice with Milli Q water using centrifuge at 4800 rpm for 10 min. The final solution was suspended in Milli Q water.

3 Results

3.1 Geometrical characterization of fabricated electrodes

Geometrical characterization of the electrodes buried in PDMS spun coated layer confirms rough topologies of the lower die. The surface roughness is mostly attributed to the FR4 (flame retardant glass reinforced epoxy laminate PCBs) sheet which gets induced through the injection molding process of the polymer. The PDMS layer although is able to smoothen the average surface roughness from 6 to 10 μm (original roughness of the as prepared FR4 sheet) (Fig. 3(c)) to 2.5–3.5 μm (roughness of the spun coated film) (Fig. 3(f)).

Figure 3 represents the reconstructed model out of profilometry data and the overall topology/surface roughness. The readout confirms the electrode width to be in the range 40–50 μm while the interelectrode gap to be in the range 50–60 μm. The surface topology of the post etched FR4 sheet is represented in (Fig. 3 (a), (b), (c) showing top view, side view and surface roughness profile respectively). The average roughness of this sheet is reported as 6–10 μm. It is obvious that the FR4 will not be affected by the etching process as the polymer is immune to the redox couple that is set up by ferric chloride. Thus it is primarily attributed to the original sheet of FR4 due to roughness induced while mold separation in the injection molding process. This can be confirmed by looking at the sidewise roughness of the PCB where there is no electroplated copper present before the etching step [See side view roughness in Fig. 3(c)]. Although the FR4 surface is smoothened a little bit with the PDMS spin coating still the overall surface topology indicates high average roughness (Fig. 3 (d), (e), (f)) ($R_a \approx 2.5$ –3.5 μm). The PDMS film spun has a thickness of 5–8 μm which is bit lower than the average surface roughness of the FR4 sheets (6–10 μm).

3.2 COMSOL simulation analysis

The surface roughness trend of 2.5–3.5 μm R_a observed from the profilometry for the whole surface is imported in the COMSOL to simulate geometrically similar microfluidic chip. Since, we are only looking at the DEP assisted capture

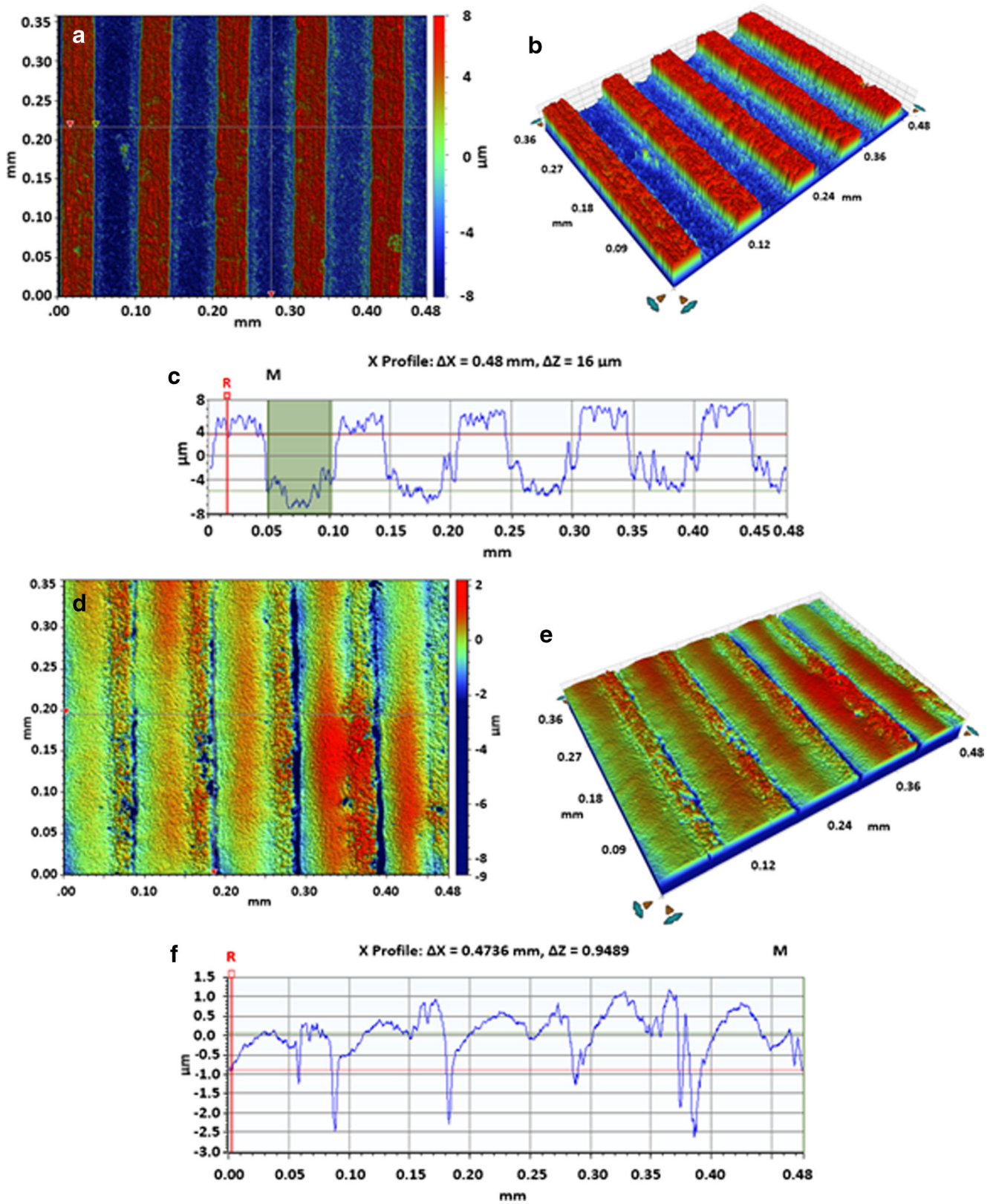


Fig. 3 Surface profile of IDEs. **a** Top view; **b** Side view; **c** surface profile before PDMS coating; **d** Top view; **e** Side view and **f** surface profile after PDMS coating

process through simulations carried out in 2-D, we have taken a 50 μm linear scan and smoothened it to get a consistent curve which reported an average roughness of 2.5 μm (300 points are borrowed to interpolate the roughness between the electrodes). We further fitted a Bezier curve based on these points to introduce 2.5 μm roughness in geometry and connected this curve at the base between two electrodes (Interelectrode gap = 55 μm). The distribution of the calculated electric field shows local enhancements over the peaks and valleys in the created roughness profile plot within the COMSOL geometry. Owing to this field concentration, the DEP capture process of the particles starts at the peaking regions and the accumulation process goes on through nucleation of capture sites at the peak regions. Figure 4 (a) and (b) shows the localization of the electric field vectors between the plane and rough surfaces respectively. Some differences have also been recorded between the maximum electric field strength in both the cases (2.5×10^6 V/m in the plane case and 5.81×10^6 V/m in the rough surface case).

In the plane surface case, the electric field concentration is mostly along the electrode corners and the interelectrode space does not possess a highly concentrated region of the electric field. However, in the rough surface case there are zones of electric field concentration particularly over the surface peaks generated due to the created roughness profile in COMSOL as described earlier. The rough topology therefore may eventually act as capture and nucleation centers for the particle collection process. The capture process is also simulated as a function of time over the plane and rough surfaces inter-connecting the electrodes and outputs are illustrated in Fig. 4(c)–(j) at different time instances for both plane and rough surface case. The outputs are recorded at time points (c)/(d) for 0 s, i.e. just before introducing the particle flow over the electrode surface (e)/(f) at $t = 1$ s, (g)/(h) at $t = 2$ s and (i)/(j) at $t = 3$ s for plane and rough surface respectively. Further each simulation output has a dual color scale, one (inner scale) representing the extent of polarizability of particle in the electric field and other (on the outer side) representing the electric field strength in that particular case. While the line color of the field lines is representative of the magnitude of the electric field the color on the particle are representative of the DEP forces faced by the particle in an electric field.

As seen in the Fig. 4 (e)/(g)/(i), corresponding to a plane interconnecting surface the capture nucleates mostly at electrode corners where the field lines have highest spatial density. On the regions away from the corners and even on the interconnecting surface there is hardly any accumulation of particles. The color patterns of the particles indicate their polarization at different zones with respect to the outlaid electrodes. The deep blue color reflects unaffected particles while the pink/red color signifies particles that are heavily influenced by the field. The trapped particles retain their position during entire capture process. In this plane surface case, the

approximate number of particles trapped at different time instances are 80 (at $t = 1$ s), 226 (at $t = 2$ s) and 397 (at $t = 3$ s) as shown in Fig. 4 (e)/(g)/(i).

While, in case of the roughness induced interconnecting surface, the approximate particles trapped at various time instances are 80 (at $t = 1$ s), 425 (at $t = 2$ s) and 694 ($t = 3$ s) as mentioned above in figure (f)/(h)/(j). Here, it is observed that roughness induced surface produces more capture of particles as compared to plane surface mostly due to high variation in the electric field and positive DEP. Due to more nucleation sites the uniformity in particle capture close to the interconnecting surface is higher in case of roughness induced topology.

For both the cases, the DEP capture comparison has been shown for first 3 s and in these 3 s, a prominent difference in capture concentration has been observed between both rough and smooth surface. In conclusion the simulations point towards a higher capture density on roughness induced surfaces owing to higher electric field gradient. The simulation results are further verified experimentally.

3.3 Experimental results

The average roughness of the FR4 surface (substrate for the PCB) FR4 is around 6–10 μm . There is no fixed pattern of the peaks and valleys between the conducting (copper) lines. Espinosa et al. 2016 has demonstrated electrodeless DEP earlier on a larger scale, where electrodes are mounted on the extreme ends of a topology in insulating material show DEP capture. The current work is about an array of regular spaced thin electrodes with an in-between spaced rough topology of an insulating surface. In a way the capture is being nucleated not only on the electrodes but also over the interconnecting insulating surface and we achieve higher capture density by utilizing both electrode assisted and electrode-less DEP over this 2-Dimensional array. The electrodes which assist the setting up of these combined phenomena should have the same order of thickness (electrode thickness ≈ 6 μm) as the induced roughness of the interconnecting surface. The coupling of both the electrode assisted and electrode-less DEP helps in taking down the magnitude of the capture voltage sufficiently, which is 10 V_{pp} in our case. Also there is an enhancement seen in the capture efficiency with this configuration. DEP assisted collection of samples (*E. coli* DH5 α stained with acridine orange at four different concentrations like 9.25×10^7 , 6.95×10^7 , 5.8×10^6 and 4.5×10^4) was carried out for duration of 1–3 h on different dilution levels of the primary sample. The occupancy due to capture was equilibrated in 5 mins in all the concentrations. Imaging of the capture area was performed in regular time intervals and the images processed were analyzed using Image-J to obtain the pixel values of the fluorescent images. The growth in fluorescence value was plotted with respect to time. A slow flow rate of 5 $\mu\text{l/h}$ is necessary to achieve higher

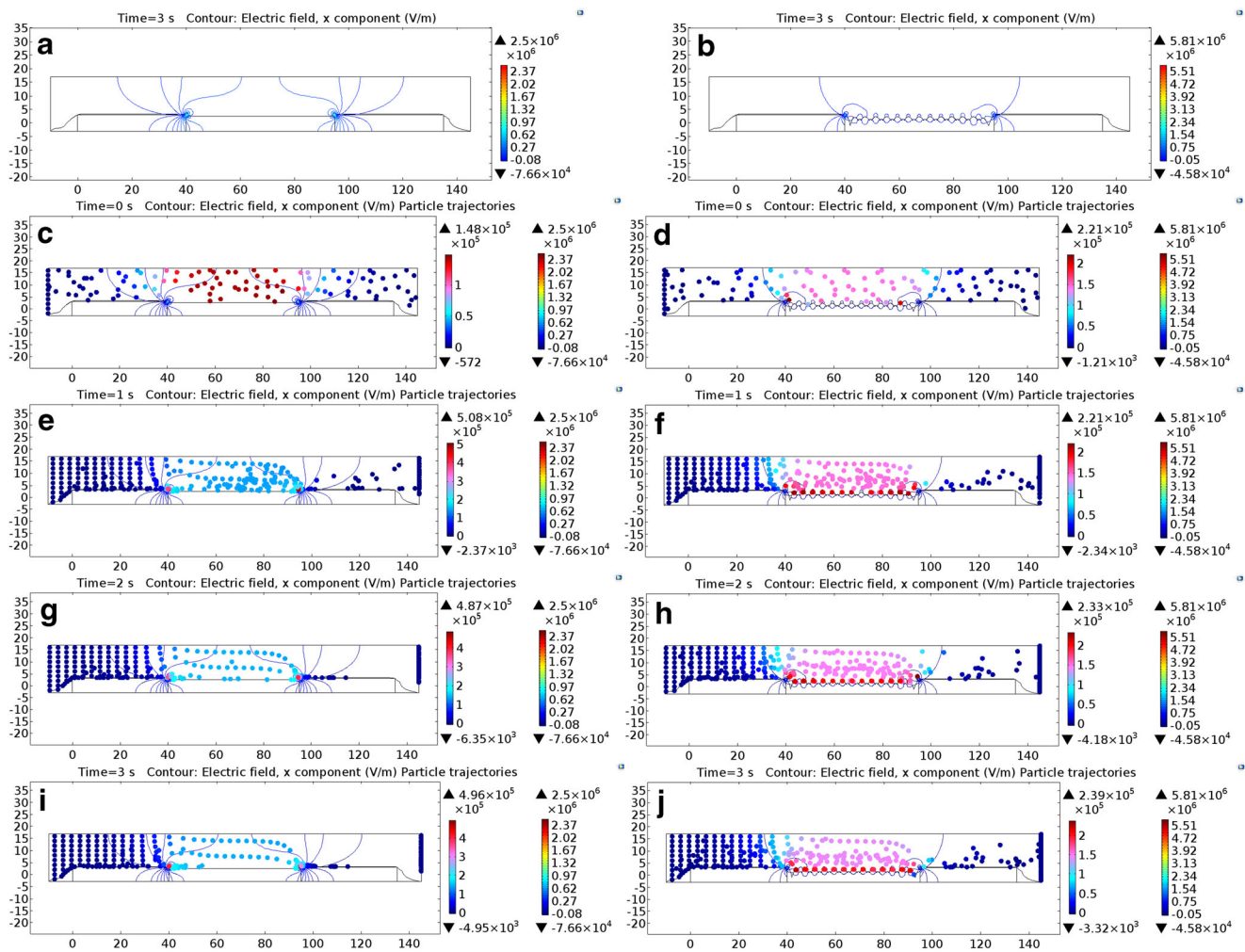


Fig. 4 Electric field pattern on electrodes. **a** plane surface; **b** with roughness; Capture with plane surface. **c** at $t = 0$ s; **e** at $t = 1$ s; **g** at $t = 2$ s; **i** at $t = 3$ s; Capture with roughness induced surface. **d** at $t = 0$ s; **f** at $t = 1$ s; **h** at $t = 2$ s; **j** at $t = 3$ s

capture efficiency. This flow rate has been achieved through a syringe pump (M/s Harvard Apparatus) using a 5 ml syringe. The capture chamber is fully flooded with the bacterial solution followed by application of the capture signal. The DEP assisted capture starts at the interelectrode regions at specific zones which are having peaks along its interconnecting surface due to roughness (Cross-sectional view (surface roughness) of the capture surface indicated in Fig. 5 (b)). The capture pattern in highlighted area (with circle-Fig. 5 (b)) is dependent of the cross-sectional roughness, higher the peak, more the capture and vice-versa. The collection is seen prominently over pleatues regions that get formulated in the interconnecting region. All imaging has been carried out at a frame rate 1 frame per sec. Figure 5 (a) ~ (h) illustrate capture images taken by

the image acquisition system at time intervals 0, 5, 15, 30, 75, 125, 180, 300 s respectively.

As can be seen in these figures the electrodes start collecting the microorganisms initially as can be seen in Fig. 5(b) and (c). Later as the electrodes are occupied with trapped microorganisms, there are specific areas along the interconnected rough surface that are observed to start collecting due to the electric field inhomogeneity. This collection can be seen to start happening from Fig. 5(c) and are seen upto Fig. 5(g) beyond which also include the secondary level peaks of lesser height etc. The phenomenon is finally able to collect over the whole domain as more time is allowed. The collection seems to happen in time over the whole surface wherever there are peaks of some specific magnitude. The fluorescence signal generated out of spot collecting dyed cells may have an associated halo effect due to which the overall brightness after 300 s may be inseparable as

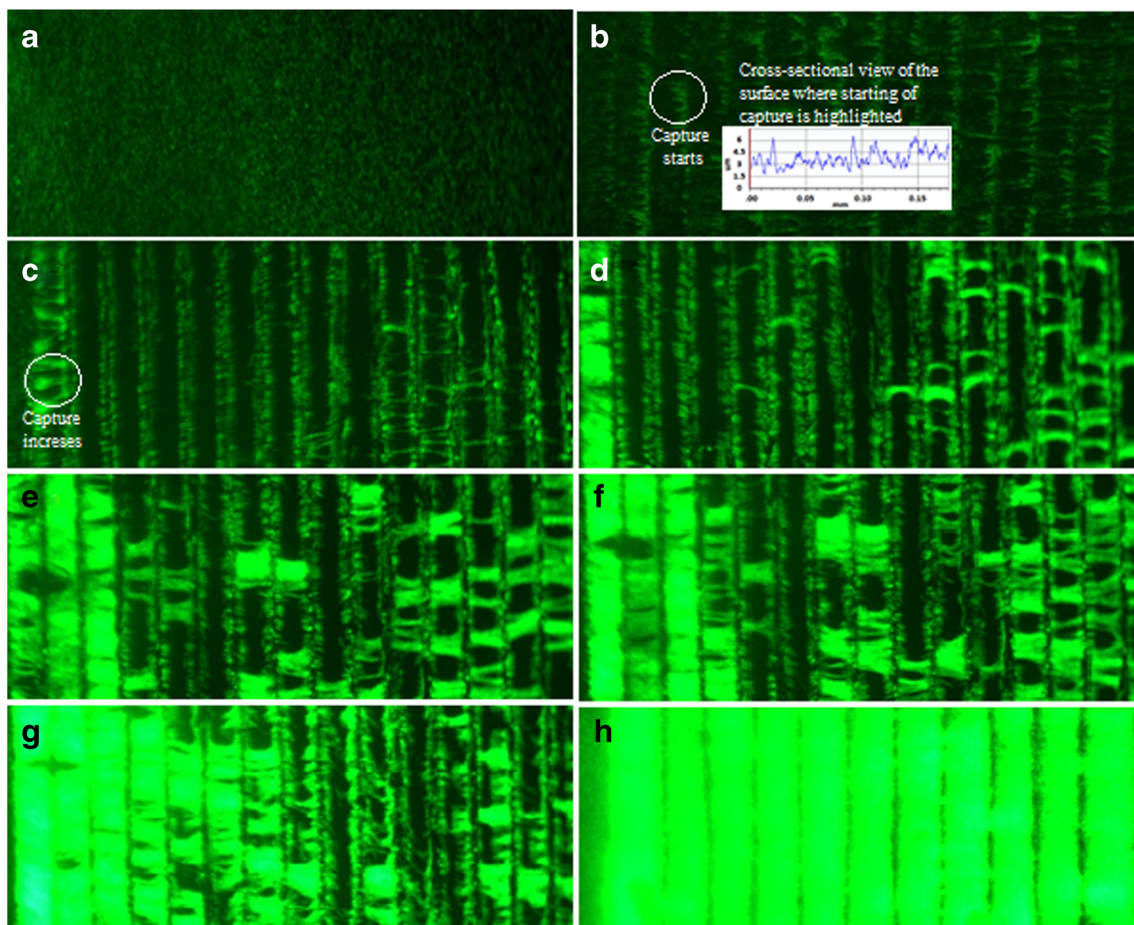


Fig. 5 DEP capture images at different instances at 9.25×10^7 cfu/ml. **a** 0 s; **b** 5 s; **c** 15 s; **d** 30 s; **e** 75 s; **f** 125 s; **g** 180 s and **h** 300 s

individual collection zones. We used the Image J analysis on the acquired images wherein the relative intensity of each image with respect to that of the image at time $t = 0$ s is plotted as a function of time. Figure 6 shows such a plot from the acquired data for different inflowing concentrations of sample solutions. It is interesting to observe a rise and pleatueing effect in the signals which has been explained well in earlier work (Ghubade et al. 2009; Nayak et al. 2013). Summarily fact which has been observed is that for a fixed concentration over a longer period of time there is an equilibrating condition (corresponding to the pleatued zone of the signal) due to interplay of the convection currents setup by the excitation source and the capture process. This results in a dynamic equilibrium wherein some sites being emptied by virtue of convention currents may be re-occupied by fresh cells which are flown into the biochip.

The studies are performed over four different concentration viz. 9.25×10^7 , 6.95×10^7 , 5.8×10^6 and 4.5×10^4 . After capture is carried out, viability studies are performed through standardized plate culture techniques and the capture efficiency is also validated using these techniques. Earlier work has also indicated that there is as such negligible viability loss in

DEP assisted collection (Nayak et al. 2013). Cell counting is performed by spreading 200 μ l of bacterial solution onto agar plates and leaving the coated plate at 37 °C for 10–12 h.

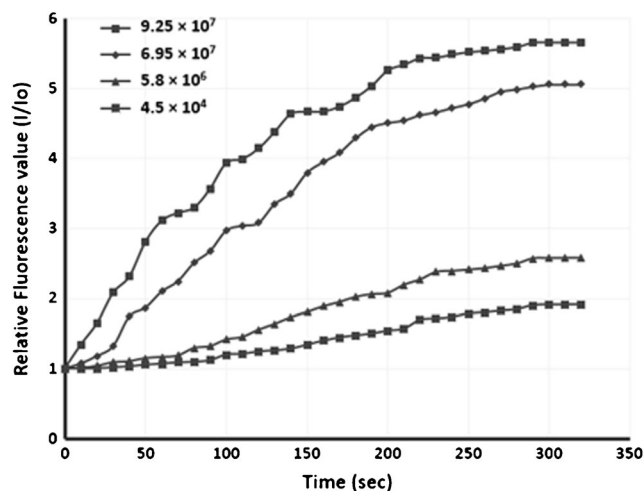


Fig. 6 Fluorescence intensity growth plot DEP capture for different concentrations; \blacksquare : 9.25×10^7 cfu/ml; \blacklozenge : 6.95×10^7 cfu/ml; \blacktriangle : 5.8×10^6 cfu/ml; \bullet : 4.5×10^4

Fig. 7 Cells plated for counting cfu/ml (9.25×10^7 cfu/ml). **a** Before DEP (10^5 dilution): 185 colonies; **b** After DEP (10^4 dilution): 264 colonies

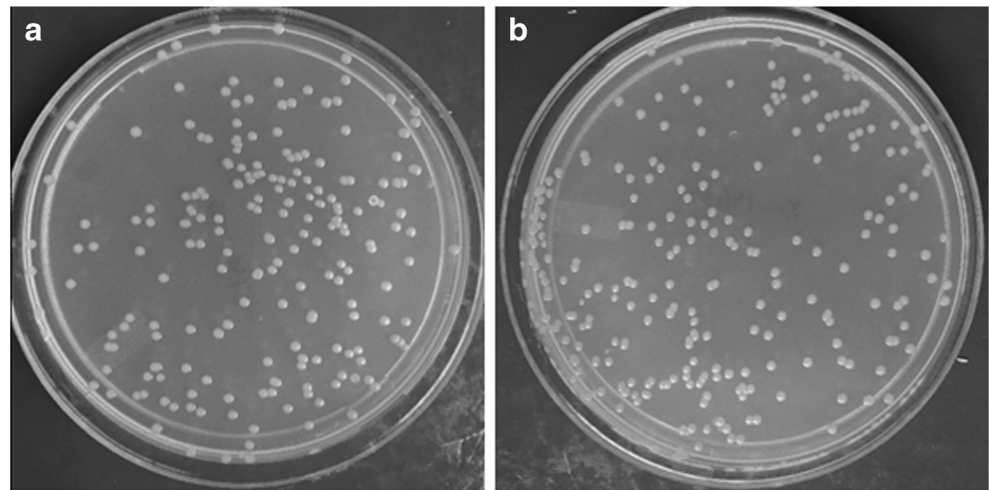


Figure 7 shows the images of the plated cells for colony counting purposes.

These colonies were counted using the ImageJ software. As shown in the figure, before DEP the the colony count was 185 at 10^5 dilution while it reached to 264 colonies at 10^4 dilution showing 85.72% efficiency of the DEP capture platform. This process was done for all the samples/concentration. The corresponding efficiency calculation was done for all the samples. Table 2 shows the efficiency corresponding to various concentrations.

Different concentrations are calculated at different concentration depending upon the countability of the plate so that it is easy to count the number of cells plated on the plate. 200 μ l volume of bacterial solution was plated for each sample to maintain the consistency in plating. From Table 2 it is observed that for different concentrations, efficiency of chip is prominently high. The maximum efficiency is achieved corresponding to 8.925×10^6 cfu/ml, i.e. 87.158%. With such a robust system, achieving this efficiency is a noble aspect. As the input voltage is very low, which facilitates DEP capture to take place, it makes the presented microfluidic chip further a more acceptable system to carry out the DEP capture based detection system.

4 Conclusion

This research concludes that the DEP is efficiently possible in PCB boards with an overall surface roughness level which may be in similar order of magnitudes as electrode thickness printed over these boards. The PCB process is a lot simpler to fabrication of hybrid biomedical platforms through lithography and other microelectronic means. The Induced roughness due to the extremely rough surface of the FR4 board accounts for DEP assisted collection over the peaking regions along the rough interconnecting surfaces. Earlier research have only indicated the DEP effect to be initiated with electrodes while overlooking of the role played by surfaces interconnecting the electrodes which this work looks in details. Additionally, the as printed IDE size on PCB has been reduced from 152 μ m (Park et al. 2009), to 40–50 μ m. Thus the collection can be initiated in this biochip of a high efficiency level (87.158%) using a low voltage 10 V_{pp} at a signal frequency 2 MHz. This chip makes an effort to realize the possibility of fabrication of lab on chip on PCB boards for diagnostics.

Table 2 Efficiency calculation corresponding to various concentrations of cells

Before DEP capture			After DEP capture			Efficiency
Cell count on plate	Dilution factor	cfu/ml	Cell count on plate	Dilution factor	cfu/ml	
185	10^5	9.25×10^7	264	10^4	1.32×10^7	85.72%
139	10^5	6.95×10^7	1785	1000	8.925×10^6	87.158%
9	1000	4.5×10^4	2	1000	1×10^4	77.777%

References

- W. Bai, K.S. Zhao, K. Asami, *Biophys. Chem.* **122**, 136–142 (2006)
- D.J. Bakewell, H. Morgan, *IEEE Trans. Nanobiosci.* **5**(1), 1–8 (2006)
- H. Chang, C.H. Chen, I.F. Cheng, C.C. Lin, Proceedings of the 2nd IEEE international conference on Nano/micro engineered and molecular systems, 1175–1178 (2007)
- C.F. Chou, J.O. Tegenfeldt, O. Bakajin, S.S. Chan, E.C. Cox, N. Darnton, R.H. Austin, *Biophys. J.* **83**(4), 2170–2179 (2002)
- M. Collet, S. Salomon, N.Y. Klein, F. Seichepine, C. Vieu, L. Nicu, G. Larrieu, *Adv. Mater.* **27**(7), 1268–1273 (2015)
- E.M. Freer, O. Grachev, X. Duan, S. Martin, D.P. Stumbo, *Nat. Nanotechnol.* **5**(7), 525–530 (2010)
- A. Ghubade, S. Mandal, R. Chaudhury, R.K. Singh, S. Bhattacharya, *Biomed. Microdevices* **11**(5), 987–995 (2009)
- B.G. Hawkins, A.E. Smith, Y.A. Syed, B.J. Kirby, *Anal. Chem.* **79**(19), 7291–7300 (2007)
- D. Ivniński, I. Abdel-Hamid, P. Atanasov, *12*(5), 317–325 (2000), doi:10.1002/(SICI)1521-4109(20000301)12:53.0.CO;2-A
- T.B. Jones, *Adv. Powder Technol.* **89** (1996)
- H. Kasahara, Z. Ding, M. Nakano, J. Suehiro, Proceedings of the IEEE international conference on industrial technology, 3341–3346 (2015)
- Y.H. Lin, G.B. Lee, *Biosens. Bioelectron.* **24**(4), 572–578 (2008)
- A. Manuscript, P.D. Instruments, NIH Public Access. **92**(1), 22–42 (2009)
- J. Mark, *Polymer Data Handbook* (Oxford Univ. Press, New York, 1999)
- E. Martinez-Salas, J.A. Martin, M. Vicente, *J. Bacteriol.* **147**(1), 97–100 (1981)
- J.C. McDonald, D.C. Duffy, J.R. Anderson, D.T. Chiu, H. Wu, O.J.A. Schueller, G.M. Whitesides, *Electrophoresis* **21**, 27–40 (2000)
- L.J. Millet, K. Park, N.N. Watkins, K.J. Hsia, R. Bashir, *JOVE J. Vis. Exp.* (48), e2545 (2011)
- M. Nayak, D. Singh, H. Singh, R. Kant, A. Gupta, S.S. Pandey, S. Mandal, G. Ramanathan, S. Bhattacharya, *Sci. Rep.* **3**, 3266 (2013)
- V. Nerguizian, A. Alazzam, D. Roman, I. Stiharu, M. Burnier, *Electrophoresis* **33**(3), 426–435 (2012)
- N.T. Nguyen, X. Huang, *Sens. Actuators A: Phys.* **88**(2), 104–111 (2001)
- K. Park, H.J. Suk, D. Akin, R. Bashir, *Lab Chip* **9**(15), 2224–2229 (2009)
- H.A. Pohl, *J. Appl. Phys.* **22**(7), 869–871 (1951)
- M.A. Saucedo-Espinosa, A. Lalonde, A. Gencoglu, M.F. Romero-Creel, J.R. Dolas, B.H. Lapizco-Encinas, *Electrophoresis* **37**(2), 282–290 (2016)
- A. Sonnenberg, J.Y. Marciniak, R. Krishnan, M.J. Heller, *Electrophoresis* **33**(16), 2482–2490 (2012)
- X.L. Su, Y. Li, *Biosens. Bioelectron.* **19**(6), 563–574 (2004)
- S. Tuukkanen, J.J. Toppari, A. Kuzyk, L. Hirviniemi, V.P. Hytönen, T. Ihalainen, P. Törma, *Nano Lett.* **6**(7), 1339–1343 (2006)
- J. Voldman, M.L. Gray, M. Toner, M.A. Schmidt, *Anal. Chem.* **74**(16), 3984–3990 (2002)
- C. Wang, K. Lan, M. Chen, M. Wang, L. Jang, *Biosens. Bioelectron.* **49**, 297–304 (2013)
- H. Wu, Y. Huang, H. Lee, W. Tsai, *Biomed. Microdevices* **2–6** (2016)